Inorganic Chemistry

Article

pubs.acs.org/IC

1:1:1 Triple-Cation B-Site-Ordered and Oxygen-Deficient Perovskite Ca_4GaNbO_8: A Member of a Family of Anion-Vacancy-Based Cation-Ordered Complex Perovskites

Tao Yang, John B. Claridge,* and Matthew J. Rosseinsky*

Department of Chemistry, University of Liverpool, Liverpool, L69 7ZD, United Kingdom

Supporting Information

ABSTRACT: Exploration of the Ca−Ga−Nb−O phase diagram by solid-state reaction in air led to isolation of Ca_4GaNbO_8. The crystal structure was determined ab initio by synchrotron X-ray and high-resolution neutron powder diffraction. Ca_4GaNbO_8 adopts a heavily distorted oxygen-deficient perovskite structure with the rare feature of complete ordering of the three B-site cations, driven by their distinct chemistries. One of the calcium cations occupies a distorted octahedral cavity and together with tetrahedrally coordinated Ga and octahedrally coordinated Nb is considered as a B-site cation in the ABO_{3-x} perovskite. This interpretation of the structure reveals Ca_4GaNbO_8 is part of a family of B-site and vacancy-ordered perovskites related to mineral structures. The anion-vacancy ordering pattern in Ca_4GaNbO_8 is driven by the coordination preferences of the three structurally distinct cations and correlated with the ordering of each cation on a distinct site. Alternating current impedance spectra show Ca_4GaNbO_8 is insulating (bulk conductivity 10^{-5}−10^{-7} S·cm^{-1}) over the measured temperature range 550−950 °C with an activation energy of 1.10(3) eV.

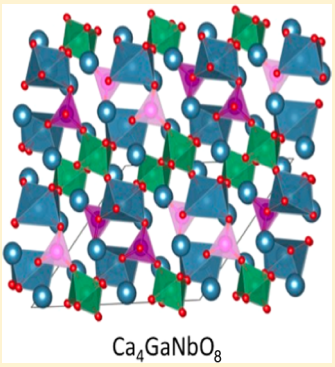

INTRODUCTION

Complex oxides have a range of functional properties determined by their compositions and the wide range of accessible structures.[1] Identification of new families of functional materials can be assisted by understanding the structural relationships between apparently diverse compounds. Control of anion defect chemistry is of particular importance in materials for solid oxide fuel cell and separation membrane applications. Oxide ion electrolytes with high conductivities, especially in the intermediate temperature range (600−800 °C), are desired for solid oxide fuel cells.[2,3] The majority of materials studied for this application contain oxide anion vacancies,[4,5] notably the fluorites $Y_xZr_{1-x}O_{2-x/2}$ and $Sm_xCe_{1-x}O_{2-x/2}$[6] and the Ga-based perovskite $La_{1-x}Sr_xGa_{1-y}Mg_yO_{3-x/2-y/2}$.[7] In the past few years, there is growing interest in systems with interstitial oxygen as the charge carrier, such as the extensively studied silicate and germinate apatites[8−11] and the gallium melilites.[12−16] In apatites, excess oxygen can be accommodated by binding to the isolated $(Si/Ge)O_4$ tetrahedral units, forming $(Si/Ge)O_5$,[17,18] while in the melilites, the interstitial oxygen moves within the 2D gallium−oxygen tetrahedral framework by forming GaO_5 units.[12,13] The motivation of the present study is to identify new complex oxides of Ga, exploiting the flexible oxide coordination characteristics of Ga^{3+}, for example, the ability to occupy environments with 4, 5, 6, or even higher oxide coordination numbers. This would make such materials suitable candidates for substitution at the non-Ga sites to modify the coordination number of Ga^{3+} and thus introduce defects into the oxide sublattice. We selected the Ca^{2+} and Nb^{5+} cations as having sufficiently different charges and bonding chemistries from Ga^{3+} to offer formation of ternary phases with distinct structural features from the known binaries. In an investigation of the Ca^{2+}−Ga^{3+}−Nb^{5+} phase diagram, a new ternary compound with composition Ca_4GaNbO_8 has been identified. Powder diffraction using synchrotron X-ray and time-of-flight neutron sources are performed to determine its crystal structure by ab initio methods. Analysis of the complex oxide network structure reveals that it is a highly distorted variant of the well-known cubic perovskite structure, featuring unusual vacancy and B-site ordering phenomena; the anion-vacancy ordering can take different forms depending on the nature of the stacking of the deficient layers. The relationship between these structures and perovskite produces an interesting set of structural relationships extending to silicate minerals and suggests several new strategies for generation of related compounds based on the ordering of three B-site cations, for which synthetic strategies are not currently well developed, and anion vacancies. Observation of a new family of perovskites based on the crystallographic order control of complex compositions opens up new synthetic opportunities.

EXPERIMENTAL SECTION

Ten samples with selected compositions were investigated in the Ca−Ga−Nb−O phase diagram (Figure S1 and Table S1, Supporting Information) by synthesis in air (1100−1225 °C). Phases Ca_4GaNbO_8 and $Ca_3Ga_{3.5}Nb_{1.5}O_{12}$[19] were observed in the ternary region of this diagram. Polycrystalline samples of the new phase Ca_4GaNbO_8 were prepared by reaction in air of stoichiometric quantites of $CaCO_3$ (Alfa

Received: November 5, 2012
Published: March 21, 2013

   dx.doi.org/10.1021/ic302414u | *Inorg. Chem.* 2013, 52, 3795−3802

Aesar 99.99%), Ga_2O_3 (Alfa Aesar 99.999%), and Nb_2O_5(Alfa Aesar 99.99%), which were ground thoroughly by hand and pressed into a 13 mm pellet. After an initial overnight calcination at 1000 °C to decompose the carbonate, the following heating sequence was used: 1200 °C−20 h, 1200 °C−20 h, 1225 °C−40 h. Further heating at 1225 °C for 60 h did not change the X-ray pattern. Between each heating step, careful regrinding and pelletizing were performed. The heating and cooling rate of the furnace was 5 °C/min. Annealed pellets were removed from the furnace below 700 °C. Long-time annealing is necessary, since $Ca_4Nb_2O_9$ forms initially and transforms to the title compound slowly, as observed by powder X-ray diffraction (XRD). A 5 g amount of Ca_4GaNbO_8 for high-resolution neutron diffraction was synthesized at 1200 °C for 70 h and 1225 °C for 40 h.

The 10 mm pellet for alternating current (ac) impedance measurements was prepared by cold-isostatic pressing (CIP) at 200 MPa, and the final step of synthesis was perfomed at 1225 °C for 60 h. The obtained pellet is 0.3502 g, with a diameter of 9.20 mm and thickness of 1.42 mm. The calculated density is 3.710 g·cm^{-3}, 92.9% of the theoretical value. Alternating current impedance spectroscopy measurements in air were performed using a Solartron 1255B frequency response analyzer coupled to a Solartron 1287 electrochemical interface over the frequency range from 10^{-2} to 10^6 Hz and the temperature range from 550 to 950 °C.

Lab powder XRD was performed on a Panalytical X'Pert Pro diffractometer using an X'Celerator detector and Co Kα1 radiation (λ = 1.78901 Å) in Bragg−Brentano geometry. Synchrotron powder XRD was carried out at Station I11 of the Diamond Light Source (λ = 0.825988 Å) at room temperature. Time of flight (TOF) neutron diffraction data were collected on the HRPD beamline at the ISIS Rutherford Appleton Laboratory. Data over the d-spacing range 0.65 Å < d < 2.59 Å were used in the Rietveld analysis with TOPAS.[20] Final reported parameters are from a combined refinement of the neutron and X-ray data (Tables 1, 2, and S2, Supporting Information).

Table 1. Crystallographic Parameters of Ca_4GaNbO_8 at Room Temperature

sample color	white
formula mass	450.95 g·mol^{-1}
space group	$P2_1/c$ (No. 14)
a/Å	11.18528(5)
b/Å	5.58787(3)
c/Å	14.07427(7)
β/deg	121.5542(2)
V/Å^3	749.606(6)
Z	4
ρ_{calcd}/g/cm^3	3.996
R_p (ND BS bank/ND 90° bank/SXRD/Total)	0.0571/0.0339/0.0459/0.0459
R_{wp} (ND BS bank/ND 90° bank/SXRD/Total)	0.0628/0.0374/0.0634/0.0551
R_{exp} (ND BS bank/ND 90° bank/SXRD/Total)	0.0362/0.0133/0.0357/0.0296
χ^2 (ND BS bank/ND 90° bank/SXRD/Total)	3.01/7.87/3.15/3.46

RESULTS AND DISCUSSION

Isolation of Ca_4GaNbO_8 was achieved following investigation of the phase diagram and optimization of the solid-state reaction conditions. The complex powder diffraction pattern was autoindexed using the Treor90 program[21] within in the software package PowderX,[22] applied to laboratory X-ray diffraction data collected in an overnight run. This afforded a monoclinic cell, $a \approx 11.190$ Å, $b \approx 5.591$ Å, $c \approx 12.593$ Å, $\beta \approx 107.67°$. The validity of the cell was confirmed by Le Bail[23] fitting using TOPAS. The extinction conditions ($h0l$: $h + l = 2n$, $0kl$: $k = 2n$, $h00$: $h = 2n$, $00l$: $l = 2n$) suggested the $P2_1/n$ space group. This was converted to the standard setting space group 14 $P2_1/c$ (Table 1). The molecular formula (Ca_4GaNbO_8) and cell volume (~750 Å^3) give Z = 4. A search of the ICSD revealed that Sr_4AlNbO_8[24] has a similar unit cell volume, but the different cell dimensions (which are accounted for later) prevent the use of this material as a model for refinement of the structure of Ca_4GaNbO_8 (Figure S2, Supporting Information).

Ab initio methods were therefore used for structure determination. Direct methods were employed by applying the program Expo to the synchrotron XRD data.[25] At the beginning, only diffraction data below 50° was used, which gave reliable independent peak intensities and proved sufficient to locate approximate positions for all metal atoms and two of the oxygen atoms. This incomplete structural model was then used in Rietveld refinement with the TOPAS software. The remaining six oxygen atoms were insensitive to X-ray diffraction and thus located from high-resolution neutron diffraction data from HRPD using the following Monte Carlo model annealing process. The coordinates of the identified atoms were first fixed; then the six extra oxygen atoms were added with random coordinates and their approximate positions located by the Monte Carlo method. Figure 1 shows the final profile fitting for the synchrotron XRD and ND patterns. Atomic coordinates, isotropic thermal displacement parameters, and selected metal−oxygen bond distances are shown in Tables 2 and 3.

There are 14 crystallographically independent atoms in the unit cell, including 4 Ca, 1 Ga, 1 Nb, and 8 O. All are located in general positions. The occupancy factors for all atoms were set free during the Rietveld refinements, and all converged to unity. The three distinct cations are thus completely ordered. Ga adopts a regular tetrahedral environment with approximately equal bond lengths, while Nb is 6-fold coordinated in an octahedral environment, where the niobium is displaced toward one face of the octahedron, affording three Nb−O distances below 2 Å. The four calcium sites Ca1−Ca4 are irregular polyhedral cavities as shown in Table 3 with coordination numbers of 7 (Ca1,Ca3) and 6 (Ca2,Ca4) (the cutoff distance used is 3 Å; the oxides not counted within the coordination polyhedra are over 3.35 Å away for Ca2 and Ca4, making their assignment of six coordination robust, whereas for Ca1 and Ca3 there are oxides at just over 3 Å separation). The mean Ca−O bond distances are 2.54 Å for Ca1, 2.44 Å for Ca2, 2.52 Å for Ca3, and 2.36 Å for Ca4. Calculated bond valence sums (BVS) for all atoms (Table 2) are consistent with expectations, with Ca1, Ca2, and Ca3 being slightly underbonded. The observed environments for each cation are shown in Figure 2. Selected bond angles for $Ca4O_6$, NbO_6, and GaO_4 are given in the Supporting Information (Table S2).

The structure is a three-dimensional framework consisting of corner-sharing CaO_6/CaO_7, NbO_6, and GaO_4 polyhedra. In order to afford clear views of the structure, only NbO_6 and GaO_4 are presented as polyhedra in Figure 3. The view along the a axis (Figure 3a) shows that the NbO_6 octahedra form zigzag chains by corner sharing. Moreover, these NbO_6 chains are decorated by alternately up- and down-oriented GaO_4 tetrahedra when viewed along the b axis. In Figure 3b, two isolated NbO_6 chains in one unit cell are presented along the c direction. The orientations of the GaO_4 tetrahedra on each polyhedral chain are the same along the a axis but alternate along c, as shown in the two distinct decorated chains shown in Figure 3b. The interchain space is occupied by the Ca^{2+}-based polyhedra.

dx.doi.org/10.1021/ic302414u | Inorg. Chem. 2013, 52, 3795−3802

Table 2. Atomic Coordinates of Ca_4GaNbO_8 at Room Temperature from Combined Refinement of Neutron and Synchrotron X-ray Data[a]

atom	site	x	y	z	U_{iso}/Å^2	BVS
Ca1	4e	0.0700(2)	0.2473(4)	0.1001(1)	0.012(2)	1.61
Ca2	4e	0.6059(2)	0.7731(4)	0.4312(1)	0.012(2)	1.85
Ca3	4e	0.7574(2)	0.2700(4)	0.1232(1)	0.012(2)	1.89
Ca4	4e	0.7098(2)	0.2309(4)	0.8598(1)	0.012(2)	2.12
Ga	4e	0.61062(9)	0.7099(2)	0.67131(8)	0.0058(3)	2.93
Nb	4e	0.92458(8)	0.7517(2)	0.63157(6)	0.0032(2)	5.09
O1	4e	0.5684(2)	0.1842(4)	0.4312(2)	0.0154(2)	1.79
O2	4e	0.0932(2)	0.8229(3)	0.1394(2)	0.0154(2)	2.10
O3	4e	0.7355(2)	0.8136(3)	0.6279(2)	0.0154(2)	1.96
O4	4e	0.3198(2)	0.1777(4)	0.1867(2)	0.0154(2)	1.85
O5	4e	0.3851(2)	0.6205(3)	0.32302(2)	0.0154(2)	1.98
O6	4e	0.0106(2)	0.0652(3)	0.7251(2)	0.0154(2)	1.85
O7	4e	0.1653(2)	0.9854(4)	0.9637(2)	0.0154(2)	2.03
O8	4e	0.8556(2)	0.9747(4)	0.5070(2)	0.0154(2)	1.93

[a]All sites are fully occupied.

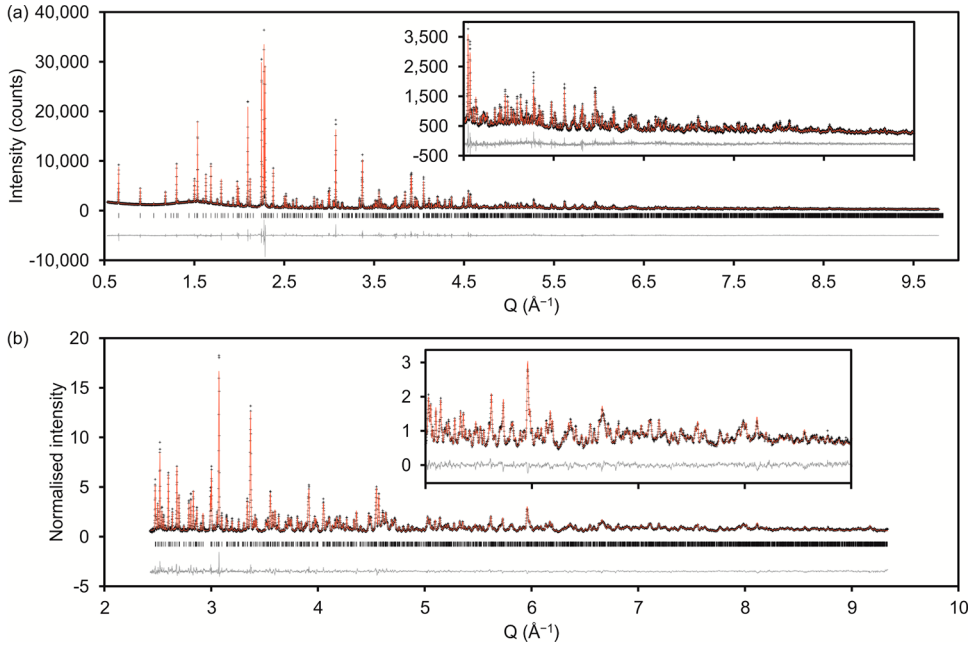

Figure 1. Rietveld refinements of Ca_4GaNbO_8 against synchrotron XRD (a) and time-of-flight neutron diffraction data (b) at room temperature. Black crosses represent observed data, and red solid line is the calculated pattern; marks below the diffraction patterns are the expected reflection positions, and difference curve is shown in gray.

The b parameter of Ca_4GaNbO_8 is similar to a $\sqrt{2}a_p$ expansion of a cubic perovskite, a_p (~4 Å), unit cell. Coupled to this, the smaller six-coordinate environment of Ca4 is a heavily distorted octahedron (Table S2, Supporting Information) and can thus be considered as a perovskite B site. Including the $Ca4O_6$ octahedra in the polyhedral representation, the view along b (Figure 4a) reveals that Ca_4GaNbO_8 can be understood as an anion-deficient perovskite with formula $Ca_3(CaGaNb)O_{9-\delta}$ ($\delta = 1$) with 3 distinct A and 3 distinct B sites. Cell parameter relationships are $a \approx 2\sqrt{2}a_p$, $b \approx \sqrt{2}a_p$, $c \approx 2\sqrt{3}a_p$, $\beta = 121.5°$ ($a = 2(a_p + b_p)$, $b = (a_p - b_p)$, $c = 2(a_p + b_p + c_p)$). The A cations Ca1, Ca2, and Ca3 are located in three distinct sites with irregular polyhedral coordination environments and significantly lower coordination numbers than the 12 coordination found in cubic perovskites (Figure 2, Table 3).

The overall structure is shown viewed along the b axis in Figure 4a. To better describe the relationship of Ca_4GaNbO_8 with perovskite, we present the polyhedral connectivity in Figure 4b and 4c along the $[001]_p$ and $[100]_p$ directions (the subscript p represent a hypothetical cubic perovskite structure). Polyhedra are corner sharing as expected for perovskite. The pattern of oxygen vacancies isolates the GaO_4 tetrahedra from each other such that one GaO_4 tetrahedron is connected to three $Ca4O_6$ and one NbO_6 octahedron. This allows the regular tetrahedral coordination favored by Ga while exploiting the ability of the more electropositive Ca to sustain a more distorted octahedral environment at Ca4. Each NbO_6 unit is connected to three $Ca4O_6$, two NbO_6, and one GaO_4 unit, while each $Ca4O_6$ is connected to three NbO_6 and three GaO_4 units. The tilt of the polyhedra along the $[001]_p$ and $[100]_p$ directions is clearly shown in Figure 4b and 4c. The direction of the previously discussed Nb^{5+} displacement from the center of the octahedral cavity is controlled by the nature of the cation neighbors, resulting in a displacement toward the Ca_4O_6 layer

dx.doi.org/10.1021/ic302414u | Inorg. Chem. 2013, 52, 3795−3802

Table 3. Bond Lengths from Combined Refinement of Neutron and Synchrotron X-ray Data of Ca_4GaNbO_8 at Room Temperature

bond	length	bond	length	bond	length
Ca1−O2	2.418(3)	Ca2−O5	2.283(3)	Ca3−O5	2.252(4)
Ca1−O6	2.422(4)	Ca2−O4	2.274(4)	Ca3−O7	2.321(3)
Ca1−O4	2.424(3)	Ca2−O1	2.335(3)	Ca3−O3	2.344(3)
Ca1−O8	2.426(4)	Ca2−O3	2.370(2)	Ca3−O1	2.420(2)
Ca1−O8	2.568(3)	Ca2−O8	2.662(3)	Ca3−O6	2.584(3)
Ca1−O7	2.637(3)	Ca2−O7	2.713(3)	Ca3−O8	2.793(4)
Ca1−O2	2.899(2)			Ca3−O2	2.863(3)
Ca4−O2	2.218(3)	Ga−O4	1.834(2)	Nb−O2	1.879(3))
Ca4−O1	2.323(4)	Ga−O1	1.849(2)	Nb−O7	1.900(2)
Ca4−O4	2.351(3)	Ga−O5	1.847(2)	Nb−O8	1.951(3)
Ca4−O5	2.363(3)	Ga−O3	1.885(3)	Nb−O6	2.036(2)
Ca4−O7	2.439(3)			Nb−O6	2.099(2)
Ca4−O8	2.474(3)			Nb−O3	2.117(3)

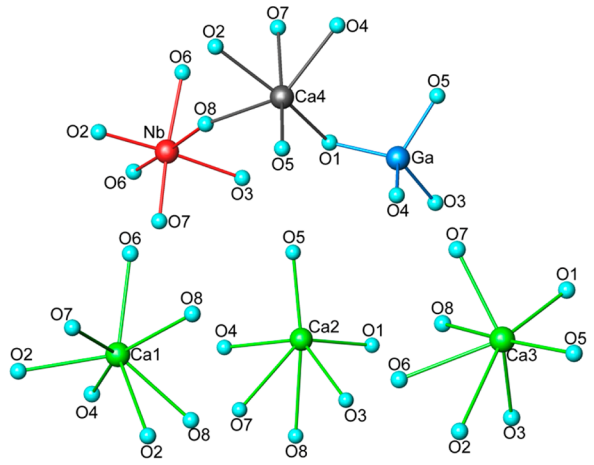

Figure 2. Coordination environments for all independent metal atoms in Ca_4GaNbO_8.

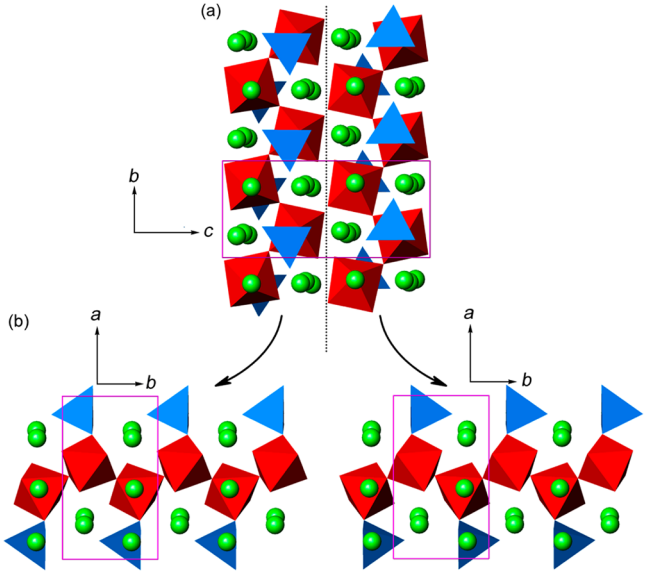

Figure 3. Structural views of Ca_4GaNbO_8 along the (a) *a* and (b) *c* axes. Two views in b correspond to two halves of the structure indicated by the dotted line in a, demonstrating the two orientations of the tetrahedra. Red and blue polyhedra are NbO_6 and GaO_4. Green spheres are Ca^{2+}. Oxygen atoms at polyhedra vertices are not explicitly shown.

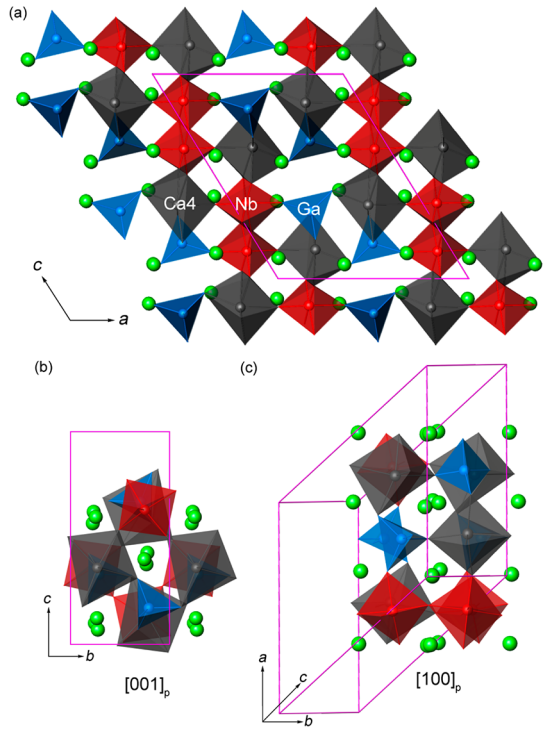

Figure 4. (a) Projected structural view along the *b* axis of Ca_4GaNbO_8. $Ca4O_6$, NbO_6, and GaO_4 are presented as gray, red, and blue polyhedra, and Ca1−Ca3 are shown as green spheres. Only part of the structure of Ca_4GaNbO_8 is shown for a better presentation of the connections between polyhedra along the (b) [001] and (c) [100] directions of a hypothetical perovskite structure. Purple solid lines represent the unit cell of the real structure.

and away from the NbO_6/GaO_4 layer approximately along $[111]_p$; such displacements are commonly seen in non-oxygen-deficient perovskites.[21] For instance, although the mean Nb−O bond length is the expected 1.99 Å, there are three short Nb−O bonds (1.872(5), 1.898(4), 1.950(4) Å) and three relatively long ones (2.033(4), 2.099(4), 2.108(4) Å). These three oxygen atoms with short Nb−O bonds belong to three neighboring $Ca4O_6$ polyhedra, so as in the Ga tetrahedral case, the presence of the flexible coordination of Ca on the octahedral site allows the geometry of Nb to be optimized while imposing a distorted coordination environment on octahedral Ca.

dx.doi.org/10.1021/ic302414u | *Inorg. Chem.* 2013, 52, 3795−3802

Having identified Ca_4GaNbO_8 as a perovskite, inspection of the reported structure of Sr_4AlNbO_8 ($P2_1/c$, a = 7.17592 Å, b = 5.80261 Å, c = 19.7408 Å, β = 97.5470°) indicates that it too is a perovskite-based material with the 1:1:1 triple B cation ordering coupled with the presence of oxygen vacancies. Cell parameter relationships in this case are $a \approx \sqrt{3}a_p$, $b \approx \sqrt{2}a_p$, $c \approx 2\sqrt{6}a_p$, β = 97.56° ($a = (a_p + b_p + c_p)$, $b = (b_p - c_p)$, $c = 2(-2a_p + b_p + c_p)$). Before dealing with the differences between these two structures and the relationship of the observed B-site cation ordering to known site-ordering patterns, it is important to relate these newly identified perovskites to established systems. Figure 5 shows that Sr_4AlNbO_8 is related to the well-known 2:1 ordered all-octahedral perovskite $Ba_3CaNb_2O_9$,[26] which has no tilting of the octahedra and ordering of Ca and Nb over the octahedral sites in layers perpendicular to the $[111]_p$ directions (Figure 5a). Removal of oxygen in an ordered manner affords Sr_4AlNbO_8, where layers of Sr-centered octahedra are separated by double layers of ordered mixed Al-centered tetrahedra and Nb-centered octahedra (Figure 5c). $Ca_4Nb_2O_9$ (Figure 5b) is a heavily distorted variant of $Ba_3CaNb_2O_9$ due to the Ca-induced tilting, reflected in the small value of the tolerance factor t = 0.85. Removal of oxygen from the $Ca_4Nb_2O_9$ structure affords Ca_4GaNbO_8 (Figure 5d), where the observed tilts can be assigned to replacement of Sr^{2+} with the smaller Ca^{2+}. Close inspection of the structures however reveals that the difference between Sr_4AlNbO_8 and $Ca_4Nb_2O_9$ is more extensive than simply the presence of tilting in the Ca case and can be assigned to the distinct chemistries of the three cations occupying the octahedral sites.

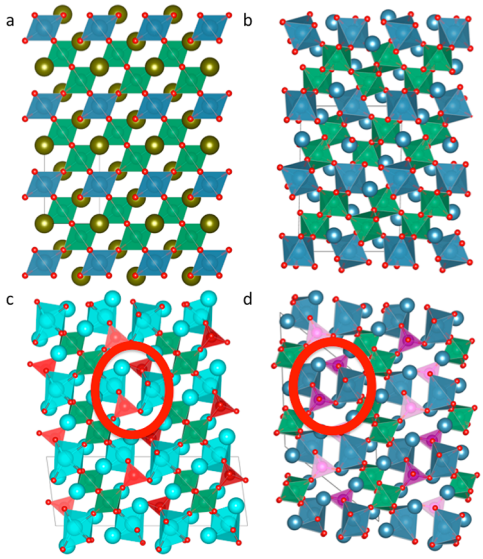

Figure 5. Structural relationships between (a) $Ba_3CaNb_2O_9$, (b) $Ca_4Nb_2O_9$, (c) Sr_4AlNbO_8, and (d) Ca_4GaNbO_8. All structures are viewed down $(1\bar{1}0)_p$ with $(111)_p$ vertical. Brown spheres are Ba, pale blue spheres are Sr, pale blue polyhedra are Sr centered, dark blue spheres are Ca, dark blue polyhedra are Ca centered, dark green octahedra are Nb centered, red tetrahedra are Al centered, and purple tetrahedra are Ga centered. Red circles highlight how the relative orientation of the polyhedra differ on opposite sides of the Ca/Sr octahedral layer.

Figure 5c and 5d compares Sr_4AlNbO_8 and Ca_4GaNbO_8 viewed along the same cubic perovskite direction. Both structures have the two ordered octahedral/tetrahedral layers separating the octahedral-only layer. The difference between Sr_4AlNbO_8 and Ca_4GaNbO_8 (highlighted in Figure 5c and 5d) derives from the arrangement of the BO_4 tetrahedra: in Ca_4GaNbO_8 the double octahedral/tetrahedral layers have the same orientations in adjacent bilayers, whereas in Sr_4AlNbO_8 the tetrahedra face in the opposite direction; this appears to be due to the coupling to the underlying octahedral tilt evidenced by the doubling of c in $Ca_4Nb_2O_9$ relative to $Ba_3CaNb_2O_9$. The tilt has different phase in successive blocks and appears to drive relaxation, which determines the tetrahedral orientation. This alternating orientation doubles the c repeat along the chains of tetrahedra in Ca_4GaNbO_8.

At the 1:1 cation ratio, there are three well-known B-site ordering types in perovskite, i.e., rock salt, columnar, and layered ordering, where B1 and B2 cations alternate in a layered fashion on the $\{111\}_p$, $\{110\}_p$, and $\{100\}_p$ planes, respectively.[27−29] In 2:1 perovskites such as $Ba_3CaNb_2O_9$, full ordering requires two distinct cations to order in [111] planes occupying the octahedral sites between AO_3 layers with a 2:1 frequency but with each layer of octahedral sites consisting of only one B cation. The B-site ordering type in the triple cation Ca_4GaNbO_8 is more complex than that of the parent compounds, because of the presence of one additional B cation, and is associated with the anion-vacancy ordering pattern as explained below. Perpendicular to the $\{111\}_p$ layers, the B cations are ordered in the sequence $Ca-(Ga_{1/2}Nb_{1/2})-(Ga_{1/2}Nb_{1/2})$. Within the $(Ga_{1/2}Nb_{1/2})-(Ga_{1/2}Nb_{1/2})$ layer, which is formed by oxygen-deficient AO_{3-x} layers to confer the tetrahedral coordination on Ga, Ga and Nb are ordered into double chains along $[110]_p$.

In order to understand the coupled anion-vacancy and cation-site ordering patterns, we consider an AO_3 layer (Figure 6a); the parent compounds arise from ordered B-cation

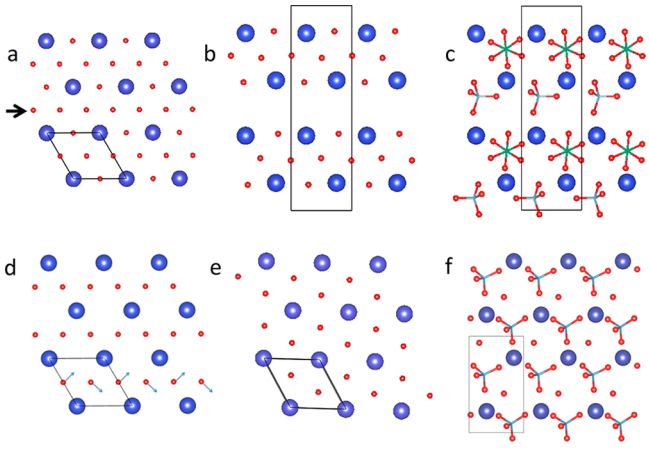

Figure 6. Removal from an AO_3 layer (a) (A blue spheres, O red spheres) of an O-only column of oxide anions (indicated by the arrow) to give the AO_2 layer found in Sr_4AlNbO_8 and Ca_4GaNbO_8 (b) which directs the Ga (cyan-centered tetrahedra) occupancy into columns in the neighboring interstitial space following the removed O; oxygens from the neighboring AO_3 layer are shown, providing three anions to the coordination sphere of both Ga and Nb. (c) Nb cations occupy the remaining (green-centered) octahedral sites, which have no anion-vacancy coordination. An alternative (d) is to remove O from an AO column followed by rearrangement (arrows) to form the more symmetrical AO_2 layer in e, which retains hexagonal coordination of A. This is commonly found in tetrahedral-only minerals such as merwinite, where the all-tetrahedral nature of the created interstitial sites is shown in f.

dx.doi.org/10.1021/ic302414u | Inorg. Chem. 2013, 52, 3795−3802

occupancy along $[111]_p$ of the octahedral sites formed by stacking these layers. This AO_3 layer can be considered as alternating AO and O_2 columns. In Ca_4GaNbO_8 and Sr_4AlNbO_8, an AO_2 layer is formed by removing alternating oxygen-only O_2 columns of oxygens along $(1-10)_p$ (Figure 6b). These AO_2 layers control the geometry of the interstitial sites occupied by the B cations. Since one-half of the O_2 columns are retained, one-half of the B cations between this AO_2 and the neighboring AO_3 layer remain in octahedral coordination: these sites are occupied by Nb. The remainder of the B sites are tetrahedral as only one O is provided by the AO_2 layer (Figure 6c) to match the three from the neighboring AO_3 layer. The columnar arrangement of the O vacancies in the AO_2 layer produces columns of tetrahedral and octahedral cations, thus coupling the anion-vacancy and cation-site order. Both trication perovskite compounds considered contain two B cations preferring octahedral coordination. Coupled with the B-site ordering, the layer stacking sequence is $AO_3-Ca-AO_3-(Ga_{1/2}Nb_{1/2})-AO_2-(Ga_{1/2}Nb_{1/2})-AO_3$. The AO_2 layer is essentially flat (Figure 7a) because of the symmetrical

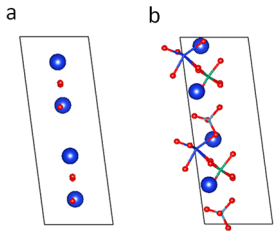

Figure 7. Contrast between the two types of A cation layer in Sr_4AlNbO_8 and Ca_4GaNbO_8. (a) Flat AO_2 layer consisting of a single crystallographic A cation site and (b) rumpled AO_3 layer consisting of two crystallographically distinct sites. Asymmetric interstitial site occupancy by the large octahedral Sr/Ca1 (bonds defining the distorted octahedron shown) and the (Ga,Al)/Nb layer (Ga tetrahedron shown) drives this buckling. Cations defining the AO_3 layer are shown as large blue spheres, Sr/Ca cations occupying the octahedral sites as small blue spheres, oxygen as red spheres, gallium/aluminum in cyan, and niobium in green.

interstitial site occupancy on either side of it by Ga and Nb, which gives the observed double chains of corner-sharing polyhedra along $(110)_p$ (Figure S3, Supporting Information). The AO_3 layer is considerably more buckled because it has an asymmetric interstitial B-site environment, with the interstitial cations on either side of this layer being different. The large (Sr or Ca) cation is located between two AO_3 layers to give an octahedral-only B layer, whereas the Ga/Nb layer is on the opposite side of the AO_3 sheet (Figure 7b). The binding of 3 anions from the AO_3 layer to complete the tetrahedral coordination at Ga drives the distortion of this layer, as only one O in the Ga coordination environment comes from the AO_2 layer. As the AO_3 layer is distorted to coordinate to Ga and thus avoid formation of terminal oxygens bound to only one cation, it affords irregular coordination at the Sr/Ca octahedral site in both materials.

An alternative more symmetric and common AO_2 layer is formed by removing all oxygen ions along AO columns along $(110)_p$ (Figure 6d). As this produces an asymmetric A cation environment, the oxygen columns then shift along $(110)_p$ to produce a hexagonal environment for the A cation in the sheets (Figure 6e), with trigonal coordination of O by A. Stacking of these AO_2 layers does not produce distinct interstitial sites for the B cations unlike the AO_2 layer discussed above; instead, the displaced O site forms regular tetrahedral environments for the interstitial B cations in combination with the AO_3 layers (Figure 6f), as observed in minerals such as merwinite[30] ($Ca_3MgSi_2O_8$) (Figure 8a) plus many other silicates, sulfates

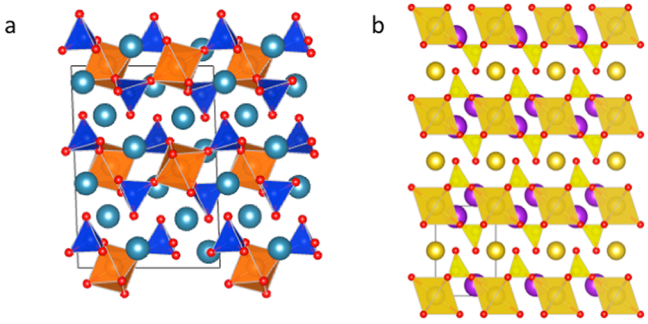

Figure 8. Merwinite (a) and apthitalite $KNaSO_4$ (b) structures derived from the more symmetrical AO_2 layer of Figure 6e viewed perpendicular to the stacking direction. Red spheres are oxygen, blue-gray spheres Ca, purple spheres K, and yellow Na. Blue and yellow tetrahedra are centered by Si and S, respectively, and brown and yellow octahedra by Mg and Na, respectively.

(e.g., apthitalite,[31] $KNaSO_4$ (Figure 8b) which, unlike merwinite, is not tilted), and related salts, as well as many hexagonal perovskites.[32] This arrangement is found when there are two cations which prefer tetrahedral coordination, e.g., the two Si in the formula unit of merwinite, and produces terminal O rather than fully condensed O in the AO_2 layers. It is possible to insert multiple perovskite blocks between the terminal tetrahedral layers.[33,34] The alternative AO_2 layer favors segregation of the B site cations into distinct layers rather than accommodation within a single layer as found for Ca_4GaNbO_8; this latter arrangement permits corner sharing of the tetrahedra and results in three-dimensional frameworks rather than the interruption of the polyhedral B-site connectivity at the terminal tetrahedral layers. The salient difference is that the columnar AO_2 layer found in Ca_4GaNbO_8 and Sr_4AlNbO_8 permits the ordered accommodation of two distinct cations in one layer of interstitial sites.

Figure 9a shows the complex impedance plots at 550, 600, and 700 °C, which comprise a single semicircular arc. This can be modeled with parallel resistor (R) and capacitance (C) elements. The intercept of the semicircular arc at low frequency is estimated as R and the capacitance estimated from $\omega RC = 1$ ($\omega = 2\pi f_{max}$, where f_{max} is the frequency corresponding to the maximum imaginary impedance) is ~1.7 pF·cm^{-1}, indicative of bulk response for the semicircular arc. At high temperatures above 800 °C, only part of the semicircular arc for the bulk response was observed. No apparent grain boundary and electrode responses were observed in the impedance data. The material shows insulating behavior (bulk conductivity 10^{-5}–10^{-7} S·cm^{-1}) over the measured temperature range 550–950 °C with an activation energy of 1.10(3) eV (see Figure 9b).

CONCLUSION

Polycrystalline Ca_4GaNbO_8 was synthesized by a solid-state reaction in air. The crystal structure was determined by synchrotron XRD and high-resolution ND. It crystallizes in the monoclinic space group $P2_1/c$ with a perovskite-related lattice: $a \approx 2\sqrt{2}a_p$, $b \approx \sqrt{2}a_p$, $c \approx 3\sqrt{6}/2a_p$, $\beta = 121.5°$. Rietveld

dx.doi.org/10.1021/ic302414u | Inorg. Chem. 2013, 52, 3795–3802

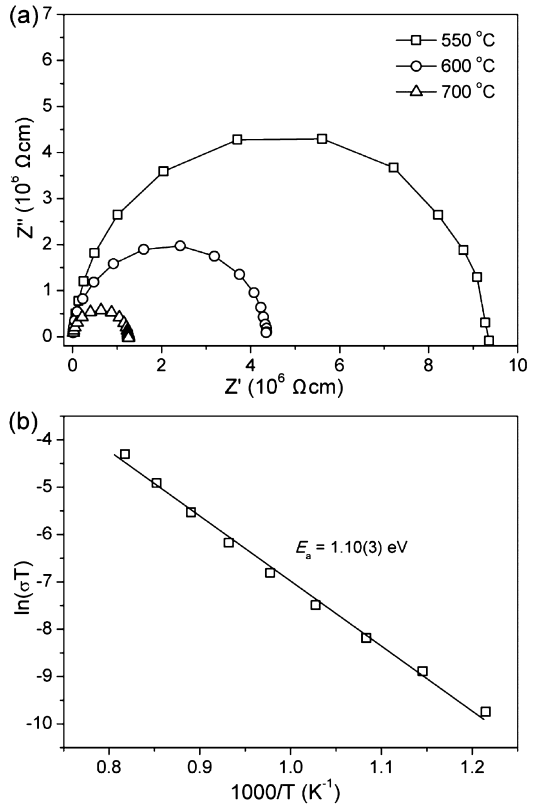

Figure 9. (a) Complex impedance plots for Ca_4GaNbO_8 at 550, 600, and 700 °C. (b) Arrhenius plot of the bulk conductivity.

refinements show it is in fact an oxygen-deficient triple perovskite, with the three Ca/Ga/Nb cations completely ordered on the B site. The ordering pattern is complex, where the sequence of the B cations on $\{111\}_p$ planes is Ca–$(Ga_{1/2}Nb_{1/2})$–$(Ga_{1/2}Nb_{1/2})$. The 2:1 arrangement of octahedral sites demonstrates the relationship with the O stoichiometric 2:1 cation-ordered phases, but the B-cation ordering pattern is more involved due to the existence of the three distinct cations coupled to columnar AO_2 vacancy order. The vacancy ordering pattern affords two arrangements of BO_4 tetrahedra exemplified by Sr_4AlNbO_8 and Ca_4GaNbO_8 due to the influence of octahedral tilting in the smaller Ca^{2+} case. In this series of triple perovskites, either with or without oxygen deficiency, A^{2+} has a wide range of sizes from Ca^{2+} to Ba^{2+} and the availability of both octahedral and tetrahedral positions for the B site may allow extension beyond the currently observed occupation by Ca^{2+}–Ga^{3+}–Nb^{5+} and Sr^{2+}–Al^{3+}–Nb^{5+}. It is feasible that the correct selection of B-site cation composition and identity in this family will result in a nonstoichiometric oxygen content of between 8 and 9. Given the low electronic conductivity, this may result in new examples of oxide ion conductors, with the observed differences in anion-vacancy ordering and polyhedral tilting potentially influencing the doping strategy to be adopted. More generally, observation of a mechanism to order three distinct B cations in the versatile perovskite structure by coupling to oxygen vacancy ordering while retaining a three-dimensional network structure opens up the synthesis of new complex functional oxides based on these motifs.

■ ASSOCIATED CONTENT

Ⓢ Supporting Information

Compositions studied in investigation of the Ca–Ga–Nb–O phase field. Bond angles in Ca_4GaNbO_8. Le Bail refinements in two candidate structures. Double chains of Ga tetrahedra in Ca_4GaNbO_8. This material is available free of charge via the Internet at http://pubs.acs.org.

■ AUTHOR INFORMATION

Corresponding Author

*E-mail: claridge@liv.ac.uk (J.B.C), m.j.rosseinsky@liverpool.ac.uk (M.J.R.).

Notes

The authors declare no competing financial interest.

■ ACKNOWLEDGMENTS

This work was supported by EPSRC under EP/H000925. We thank Dr. P. A. Chater for assistance with the combined refinement.

■ REFERENCES

(1) Rao, C. N. R.; Raveau., B. *Transition Metal Oxides: Structure, properites and synthesis of ceramic oxides*, 2nd ed.; VCH-Wiley: New York, 1998.
(2) Steele, B. C. H.; Heinzel, A. *Nature* **2001**, *414*, 345.
(3) Goodenough, J. B. *Annu. Rev. Mater. Res.* **2003**, *33*, 91.
(4) Boivin, J. C.; Mairesse, G. *Chem. Mater.* **1998**, *10*, 2870.
(5) Lacorre, P.; Goutenoire, F.; Bohnke, O.; Retoux, R.; Laligant, Y. *Nature* **2000**, *404*, 856.
(6) Hull, S. *Rep. Prog. Phys.* **2004**, *67*, 1233.
(7) Huang, K. Q.; Tichy, R. S.; Goodenough, J. B. *J. Am. Ceram. Soc.* **1998**, *81*, 2565.
(8) Nakayama, S.; Kageyama, T.; Aono, H.; Sadaoka, Y. *J. Mater. Chem.* **1995**, *5*, 1801.
(9) Leon-Reina, L.; Losilla, E. R.; Martinez-Lara, M.; Bruque, S.; Aranda, M. A. G. *J. Mater. Chem.* **2004**, *14*, 1142.
(10) Islam, M. S.; Tolchard, J. R.; Slater, P. R. *Chem. Commun.* **2003**, 1486.
(11) Arikawa, H.; Nishiguchi, H.; Ishihara, T.; Takita, Y. *Solid State Ionics* **2000**, *136*, 31.
(12) Kuang, X.; Green, M. A.; Niu, H.; Zajdel, P.; Dickinson, C.; Claridge, J. B.; Jantsky, L.; Rosseinsky, M. J. *Nat. Mater.* **2008**, *7*, 498.
(13) Li, M.-R.; Kuang, X.; Chong, S. Y.; Xu, Z.; Thomas, C. I.; Niu, H.; Claridge, J. B.; Rosseinsky, M. J. *Angew. Chem., Int. Ed.* **2010**, *49*, 2362.
(14) Thomas, C. I.; Kuang, X.; Deng, Z.; Niu, H.; Claridge, J. B.; Rosseinsky, M. J. *Chem. Mater.* **2010**, *22*, 2510.
(15) Liu, B.; Ding, D.; Liu, Z.; Chen, F.; Xia, C. *Solid State Ionics* **2011**, *191*, 68.
(16) Wei, F.; Baikie, T.; An, T.; Schreyer, M.; Kloc, C.; White, T. J. *J. Am. Chem. Soc.* **2011**, *133*, 15200.
(17) Sansom, J. E. H.; Tolchard, J. R.; Islam, M. S.; Apperley, D.; Slater, P. R. *J. Mater. Chem.* **2006**, *16*, 1410.
(18) Pramana, S. S.; Klooster, W. T.; White, T. J. *Acta Crystallogr., Sect. B: Struct. Sci.* **2007**, *63*, 597.
(19) Shimamura, K.; Timoshechkin, M.; Sasaki, T.; Hoshikawa, K.; Fukuda, T. *J. Cryst. Growth* **1993**, *128*, 1021.
(20) *TOPAS, V4.1-academic*; Bruker AXS: Karlsruhe, Germany, 2004.
(21) Werner, P. E.; Eriksson, L.; Westdahl, M. *J. Appl. Crystallogr.* **1985**, *18*, 367.
(22) Dong, C.; Wu, F.; Chen, H. *J. Appl. Crystallogr.* **1999**, *32*, 850.
(23) Le Bail, A.; Duroy, H.; Fourquet, J. L. *Mater. Res. Bull.* **1988**, *23*, 447.
(24) Lee, E.; Hong, S.-T. *J. Solid State Chem.* **2008**, *181*, 2930.

(25) Altomare, A.; Burla, M. C.; Camalli, M.; Carrozzini, B.; Cascarano, G. L.; Giacovazzo, C.; Guagliardi, A.; Moliterni, A. G. G.; Polidori, G.; Rizzi, R. *J. Appl. Crystallogr.* **1999**, *32*, 339.
(26) Deng, J.; Chen, J.; Yu, R.; Liu, G.; Xing, X. *J. Alloys Compd.* **2009**, *472*, 502.
(27) Anderson, M. T.; Greenwood, K. B.; Taylor, G. A.; Poeppelmeier, K. R. *Prog. Solid State Chem.* **1993**, *22*, 197.
(28) King, G.; Woodward, P. M. *J. Mater. Chem.* **2010**, *20*, 5785.
(29) Davies, P. K.; Wu, H.; Borisevich, A. Y.; Molodetsky, I. E.; Farber, L. *Annu. Rev. Mater. Res.* **2008**, *38*, 369.
(30) Moore, P. B.; Araki, T. *Am. Mineral.* **1972**, *57*, 1355.
(31) Bellanca, A. *Period. Mineral.* **1943**, *14*, 67.
(32) Darriet, J.; Subramanian, M. A. *J. Mater. Chem.* **1995**, *5*, 543.
(33) Kuang, X. J.; Claridge, J. B.; Price, T.; Iddles, D. M.; Rosseinsky, M. J. *Inorg. Chem.* **2008**, *47*, 8444.
(34) Bendraoua, A.; Quarez, E.; Abraham, F.; Mentre, O. *J. Solid State Chem.* **2004**, *177*, 1416.